Astron. Astrophys. 320, 65–73 (1997)

ASTRONOMY
AND
ASTROPHYSICS

Chaos, complexity, and short time Lyapunov exponents: two alternative characterisations of chaotic orbit segments

Henry E. Kandrup[1,2], **Barbara L. Eckstein**[1], **and Brendan O. Bradley**[3]

[1] Department of Astronomy, University of Florida, Gainesville, FL 32611, USA
[2] Department of Physics and Institute for Fundamental Theory, University of Florida, Gainesville, FL 32611, USA
[3] Department of Mathematics, University of New Mexico, Albuquerque, NM 87131, USA
(kandrup@astro.ufl.edu; eck@astro.ufl.edu; brendan@math.unm.edu)

Received 20 May 1996 / Accepted 17 September 1996

Abstract. This paper compares two tools useful in characterising ensembles of chaotic orbit segments in a time-independent galactic potential, namely Fourier spectra and short time Lyapunov exponents. Motivated by the observation that nearly regular orbit segments have simpler spectra than do wildly chaotic segments, the *complexity* $n(k)$ of a discrete Fourier spectrum, defined as the number of frequencies that contain a fraction k of the total power, is identified as a robust quantitative diagnostic in terms of which to classify different chaotic segments. Comparing results derived from such a classification scheme with the computed values of short time Lyapunov exponents shows that there is a strong, often nearly linear, correlation between the complexity of an orbit and its sensitive dependence on initial conditions. Chaotic segments characterised by complex Fourier spectra tend systematically to have a larger maximum short time Lyapunov exponent than do segments with simpler spectra. It follows that the distribution of complexities, $N[n(k)]$, associated with an ensemble of chaotic segments of length Δt can be used as a diagnostic for phase space transport in much the same way as the distribution of maximum short time Lyapunov exponents, $N[\chi]$, associated with the same ensemble.

Key words: galaxies: kinematics and dynamics – chaos

1. Introduction and motivation

Generic N degree of freedom Hamiltonian systems characterised by time-independent potentials typically admit a coexistence of both regular and chaotic orbits. Thus, e.g., the constraint of fixed energy E (and any other isolating integrals) restricts evolution to a lower-dimensional hypersurface in the $2N$-dimensional phase space which, in many cases, will contain one or more regular islands embedded in a surrounding stochastic sea. Moreover, one discovers oftentimes that the stochastic sea is connected in the sense that a single chaotic orbit will, in a $t \to \infty$ limit, pass arbitrarily close to every point in the sea.

This leads to the expectation that, at sufficiently late times, different chaotic orbits in a connected phase space region will all exhibit the same statistical properties (cf. Lichtenberg & Lieberman 1992). However, one knows that finite segments of different, or even the same, chaotic orbits can look extremely different from one another: sometimes a segment will look wildly chaotic; sometimes it may be nearly indistinguishable from a regular orbit. At least in part, this diversity in visual appearance is associated with partial phase space obstructions like cantori (cf. Aubry & Andre 1978, Mather 1982) or an Arnold web (Arnold 1964) that partition the space into regions which, albeit not completely disjoint, may only communicate on relatively long time scales.

One way in which to characterise the sense in which a given chaotic segment is nearly regular or wildly chaotic is to determine the complexity of the Fourier spectrum. Regular orbits have spectra where (at least for sufficiently large t) power is concentrated near a discrete set of frequencies. Chaotic orbits tend to exhibit broader band power. In particular, the spectrum associated with a long time integration typically appears to be continuous, with significant power for a broad range of frequencies (cf. Tabor 1989). However, the spectra associated with shorter time segments exhibit considerable diversity. Sometimes the spectrum looks exceedingly simple, with almost all the power concentrated at a few special frequencies, whereas in other cases the spectrum appears more complex, with significant power at a relatively large number of frequencies. Moreover, there is a clear sense in which the "most complex" spectra correlate with orbit segments that look the most wildly chaotic.

Another way to characterise a chaotic segment is by computing short time Lyapunov exponents $\chi(\Delta t)$, which (cf. Grassberger et al. 1988, Sepúlveda et al 1989) probe the average degree of exponential instability over a finite time interval Δt. Visually, it seems that segments for which the maximum short time exponent is especially large tend to look particularly chaotic,

Send offprint requests to: H.E. Kandrup (Florida Astronomy)

whereas smaller maximum exponents correlate with segments that appear more nearly regular. In particular, a distribution of maximum short time Lyapunov exponents, $N[\chi(\Delta t)]$, computed for an ensemble of orbits in the same connected phase space region, some of which are trapped near regular islands and others of which travel throughout the remaining stochastic sea, typically looks as if it is generated as a sum of two or more distinct populations (Mahon et al 1995).

The aim here is to quantify the degree to which these two different characterisations of chaos – the complexity of a Fourier spectrum and the value of the maximum short time Lyapunov exponent – agree when used to classify chaotic orbit segments.

2. The invariant spectrum of chaos

A single chaotic initial condition evolved in a time-independent potential for sufficiently long times will eventually sample an invariant measure, or distribution, Γ. Moreover, if an ensemble of initial conditions, each corresponding to a chaotic orbit in the same connected phase space region, is evolved into the future it will typically exhibit a coarse-grained evolution towards this same invariant Γ (cf. Kandrup & Mahon 1994a).

It is not surprising that the invariant measure Γ associated with any connected chaotic phase space region is characterised by invariant distributions of short time Lyapunov exponents and invariant Fourier spectra. If, for a fixed time interval Δt, a distribution of short time exponents is computed for a collection of Q initial conditions that samples the invariant measure, the resulting $N[\chi(\Delta t)]$ will assume a unique form which, modulo finite number statistics, is independent of the detailed choice of initial conditions, although it *can* depend sensitively on the length of the interval Δt (Kandrup & Eckstein 1996). Similarly, the Fourier spectrum extracted from an integration of Q different initial conditions that sample the invariant measure depends only on the connected phase space region that is being sampled, again independent of the detailed choice of initial conditions (Kandrup & Bradley 1995).

In extracting an invariant Fourier spectrum of chaos from a sampling of the invariant measure, it seems natural to (i) integrate each initial condition for a fixed time interval Δt, sampling at uniformly spaced intervals δt, (ii) compute the power spectra, $|x_j(\omega)|^2$ and $|y_j(\omega)|^2$ for each individual segment j, and then (iii) identify composite spectra such as

$$|x(\omega)|^2 = \frac{1}{Q}\sum_{j=1}^{Q}|x_j(\omega)|^2. \tag{1}$$

If the sampling interval Δt is too short, such a prescription will miss significant contributions at frequencies $\omega < 2\pi/(\Delta t)$. If, however, the resulting spectrum has its power concentrated away from $\omega \to 0$, one can be reasonably confident that the spectra capture most of the intrinsic periodicities. In any event if, as is the case here, one selects Δt as corresponding to the Hubble time t_H, any lost periodicities reflect effects which proceed on time scales $> t_H$ which, arguably, are physically irrelevant.

That different initial conditions in the same connected phase space region converge towards the same invariant power spectra can be demonstrated explicitly by computing the "distance" between their spectra, as defined with respect to some norm. Thus, e.g., given two spectra, $|x_1(\omega)|$ and $|x_2(\omega)|$, one can define a discrete L^p norm, $D_p x_{12}$, by the expression

$$D_p x_{12} = \Big(\sum_{\alpha}\big||\hat{x}_1(\omega_\alpha)| - |\hat{x}_2(\omega_\alpha)|\big|^p\Big)^{1/p}, \tag{2}$$

where α labels the discrete frequencies and

$$|\hat{x}(\omega_\alpha)| = \frac{|x(\omega_\alpha)|}{\sum_\alpha |x(\omega_\alpha)|}.$$

This construction is well defined for all $p > 0$, but restriction here has focused on the special cases $p = 1$ and $p = 2$, which seem especially well motivated physically.

If two different initial conditions in the same connected phase space region are integrated for a total time $Q\Delta t$, and their spectra computed as in Eq. (1), one discovers generically that, for sufficiently large Q, $D_p x_{12} \ll 1$. However, as will be evident from the discussion in Sect. 3 (cf. Fig. 4), the time required to achieve a reasonable convergence can vary enormously, depending, e.g., on the extent to which the phase space is partitioned by cantori or other topological semi-obstructions. Similarly, if one samples the invariant measure to generate two different random sets of Q initial conditions, evolves all the initial conditions in each set for a time Δt, and then computes composite spectra, $|x_1(\omega)|$ and $|x_2(\omega)|$, one finds that, within statistical uncertainties, $D_p x_{12} \approx 0$.

As a practical matter, a collection of chaotic segments sampling the invariant measure can be generated in a number of different ways. The most obvious computationally, albeit not necessarily the most efficient, is to integrate a single initial condition for a very long time $Q\Delta t$ and then partition the resulting time series into a collection of Q segments of length Δt. In this connection, it should be noted that performing a Fourier transform of the entire orbit segment is much more expensive computationally, and provides no more information, than transforming the Q partitioned segments. It might seem that, by working directly with the full orbit, one can obtain information about Q times as many frequencies. However, to extract equally meaningful results one needs to average over collections of Q adjacent frequencies, at which point one recovers essentially the same information as extracted from the Q individual segments (cf. p. 552 in Press et al. 1992).

The results described in this paper involve the choice of a basic sampling time $\Delta t \approx t_H$. Three different two-dimensional potentials were considered. The first two, the so-called dihedral potential of Armbruster et al. (1989) and the sixth order truncation of the three-particle Toda lattice potential (Toda 1967) are well known to the nonlinear dynamicist. The third potential, perhaps more realistic from the viewpoint of the galactic dynamicist, is given (cf. Mahon et al. 1995) as the sum of an

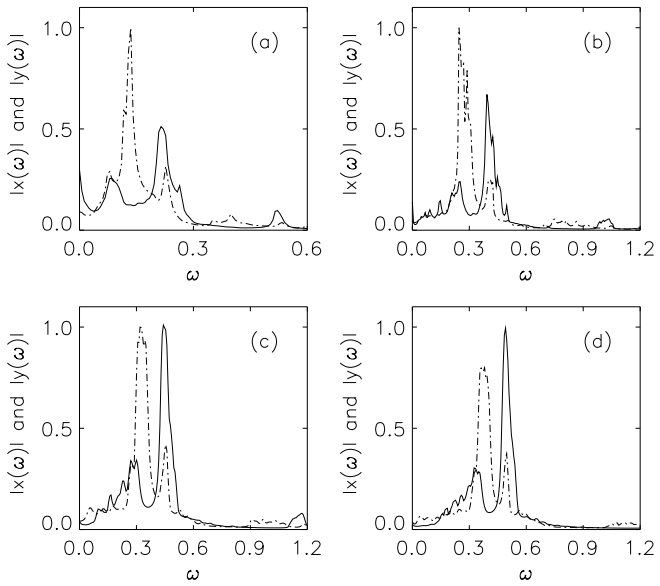

Fig. 1. a The invariant Fourier spectra, $|x(\omega)|$ and $|y(\omega)|$, for chaotic orbits with energy $E = -0.3$, evolved in the potential (3). $|x(\omega)|$ is represented by a solid curve and $|x(\omega)|$ by a dot-dashed curve. **b** The same for $E = -0.5$. **c** The same for $E = -0.55$. **d** The same for $E = -0.6$.

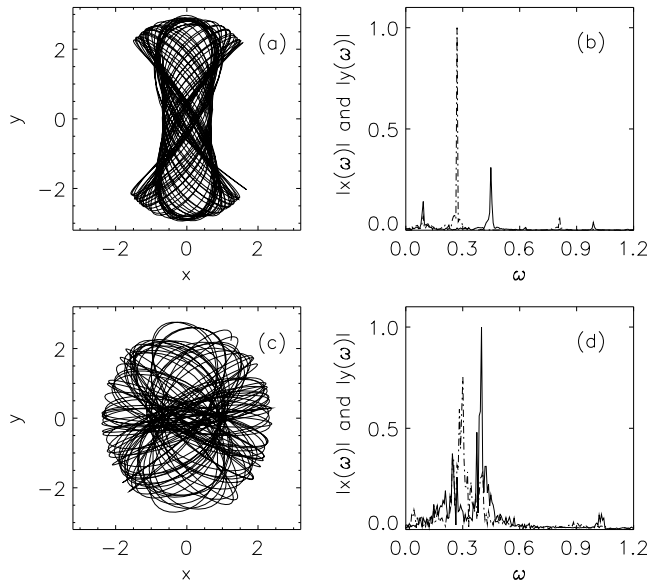

Fig. 2. a The configuration space $x - y$ trajectory for one chaotic orbit segment with $E = -0.5$ evolved for a time t_H in the potential (3).**b** The Fourier spectra, $|x(\omega)|$ and $|y(\omega)|$, for the segment in the preceding panel. **c** Another chaotic segment with $E = -0.5$ evolved in the same potential for the same total time. **d** The Fourier spectra for the segment in the preceding panel.

isotropic Plummer potential and an anisotropic Plummer potential. Specifically,

$$V(x,y) = -\frac{1}{(1+x^2+y^2)^{1/2}} - \frac{m}{(1+x^2+ay^2)^{1/2}}, \qquad (3)$$

with $a = 0.1$ and $m = 0.3$. The principal conclusions derived from the three different potentials are essentially identical, so that explicit attention here will focus primarily on the last potential. For reasonable energies in this potential, a typical crossing time corresponds to $t \sim 10$, so that one can identify $\Delta t = t_H = 1024$. Orbits integrated in this potential were sampled at intervals $\delta t = 1/2$, this leading to a Fourier spectrum with power at 2048 different frequencies (cf. Press et al. 1992).

Invariant spectra were generated for a number of different energies, in each case by analysing 16 different initial conditions evolved for a time $128t_H$, this resulting in 2048 segments of length t_H.[1] The choice of initial conditions was based on carefully computed surfaces of section (cf. Kandrup & Bradley 1995, Mahon et al. 1995) and corresponded to phase space points displaced from any regular islands. Because of the long duration of the integrations, $t = 128t_H$, the specific choice of initial conditions is unimportant, provided only that the initial conditions correspond to chaotic orbits. The results for four representative energies, $E = -0.3$, -0.5, -0.55, and -0.6, are exhibited in Figs. 1. As inferred from a surface of section, the chaotic phase space at $E = -0.3$ is relatively large and, over time scales as long as t_H, cantori are unimportant. For the lower energies, cantori play an increasingly important role. In each panel, $|x(\omega)|$ is given by a solid curve and $|y(\omega)|$ by a dot-dashed curve. The overall normalisation in each panel was fixed by the demand that the peak amplitude of the larger of $|x(\omega)|$ and $|y(\omega)|$ be equal to unity.

It is clear that these spectra are relatively broad band, characterised to the level of resolution by significant power for a continuous set of frequencies. However, it is equally clear that these invariant spectra manifest a significant amount of structure. Although these spectra differ greatly from those associated with regular orbits, they *are* similar in that the typical values of ω where most of the power is concentrated are comparable for both regular and chaotic orbits. Moreover, there is a real sense in which the overall shape of the spectra can be viewed as reflecting contributions from different regular orbits that exist at the same energy (cf. Kandrup & Bradley 1995). In particular, it is easy to mimic the shape of the invariant spectrum by allowing only for a relatively small number of regular loops, boxes, and bananas.

Consider, e.g., the spectra for $E = -0.3$. Here the peaks at $\omega \approx 0.08$ and 0.22 common to both $|x(\omega)|$ and $|y(\omega)|$ reflect contributions from loops, whereas the peak in $|y(\omega)|$ at $\omega \approx 0.12$ is associated with boxy contributions. The peak at $\omega \to 0$ for $|x(\omega)|$ is associated with the existence of a large measure of regular banana orbits.

That the invariant Fourier spectra can be interpreted as reflecting "pieces" of different regular orbits is not unreasonable

[1] For example, for $E = -0.3$ the initial conditions were $(x, y, p_y) =$ (0.06, 4.63, 0.13), (0.20, 4.00, 0.00), (0.24, 3.85, 0.17),(0.30, 3.40, 0.20), (0.45, 5.45, 0.20), (0.80, 3.40, 0.20), (0.85, 3.30, 0.11), (1.26, 0.13, 0.89), (1.30, 0.66, 0.64), (1.82, 4.41, 0.21), (1.88, 3.64, 0.29), (1.90, 4.09, 0.26), (2.12, 2.52, 0.33), (2.61, 3.27, 0.18), (3.00, 0.50, 0.10), and (3.60, 0.45, 0.20), with $p_x = p_x(x, y, p_y, E) > 0$.

given the fact that, in certain cases, short time segments of a chaotic orbit can look very regular. Moreover, even for a wildly chaotic segment one can often identify various features which one would like qualitatively to interpret as "boxy" or "loopy." This idea is also eminently plausible given the interpretation of chaos as arising from resonance overlap. If, e.g., one attempts to approximate an invariant spectrum as a sum of several different regular orbits, he or she will discover typically that the resulting collection will involve both boxes and loops with appreciable power at or near the same frequency. In this connection, it should be stressed that the dip in $|y(\omega)|$ at $\omega \approx 0.27$ for $E = -0.5$ is almost certainly real, and that the apparent broad peak in $y(\omega)$ seems comprised of a lower peak reflecting loopy contributions and a higher peak reflecting boxy contributions.

3. The complexity of chaotic orbit segments

Regular orbits look simple visually since, being multiply periodic, they close on themselves. Their Fourier spectra are characterised by a small number of sharply defined peaks corresponding to certain fundamental frequencies and various harmonics thereof. By contrast, chaotic orbits integrated for a long time look complex because they are aperiodic and, as such, are characterised by Fourier spectra which have significant power at a relatively large number of frequencies. Given these observations, it seems natural to characterise the degree of chaos exhibited in a finite segment of a chaotic orbit by determining the overall *complexity* of the Fourier spectrum. A chaotic segment that looks "nearly regular" will typically have a spectrum that is nearly indistinguishable from that of a regular orbit, whereas a "wildly chaotic" segment will exhibit significant power at a relatively large number of frequencies.

This notion of complexity is connected with the problem of compression, i.e., the degree to which the information content of an orbit can be encapsulated, at least approximately, by a relatively small number of basis functions. If some segment is wildly chaotic, one must retain a large number of coefficients in a Fourier expansion if the inverted expansion is to yield a decent approximation to the original orbit. If the segment is nearly regular, a smaller number of coefficients will suffice. Suppose, e.g., that a time series $x(t_i)$ ($i = 1, ..., m$) is transformed into a Fourier series $x(\omega_i)$ using a standard *FFT* routine (cf. Press et al. 1992) and that the resulting $x(\omega_i)$ is then subjected to a filter which identifies the smallest set of j frequencies which contain a fraction k of the total power, $\sum_i |x(\omega_i)|^2$, and sets $x(\omega_i) \equiv 0$ for all the remaining frequencies. It then follows from Parseval's Theorem that the reconstructed time series $x_R(t_i)$ generated from the j special frequencies will satisfy

$$\|x - x_R\| \equiv \left(\sum_{i=1}^{m} |x(t_i) - x_R(t_i)|^2 \right)^{1/2} \leq \epsilon \left(\sum_{i=1}^{m} |x(t_i)|^2 \right)^{1/2}$$

$$\equiv \epsilon \|x\|, \qquad (4)$$

where $\epsilon = (1 - k)^{1/2}$.

Motivated by the preceding observations, a quantitative characterisation of the complexity of a two-dimensional chaotic orbit segment, $n(k)$, can be defined as follows: For a given threshold k, identify $n_x(k)$ and $n_y(k)$ as the numbers of frequencies required to capture, respectively, a fraction k of the total x- and y-powers. Then set $n(k) = n_x(k) + n_y(k)$.

If such a prescription is to be reasonable, one needs to determine the "right" choice of k or, even better, to show that the results of such a classification scheme are relatively insensitive to the precise value of k that is used. In fact, it was found that values of k between 0.6 and 0.95 yield quite similar results. This can be quantified by computing the complexity for each member of an ensemble of segments for several values of k and then calculating a rank correlation, $\mathscr{R}(k_1, k_2)$, between the results obtained for two different choices, k_1 and k_2. For a variety of energies and potentials, it was found that for segment lengths $\sim 0.5 - 2t_H$, the typical rank correlation $\mathscr{R}(0.6, 0.95) \sim 0.8$, the worst case corresponding to $\mathscr{R} \sim 0.6$. Similarly, the typical $\mathscr{R}(0.7, 0.9) \sim 0.9$, the worst case here corresponding to $\mathscr{R} \sim 0.8$.

But what is the "right" choice of k? Smaller values of k are comparatively insensitive diagnostics, since the range of $n(k)$'s exhibited by different segments is relatively small. However, values of k that are too large also seem unsatisfactory: Because the orbit segments are of finite length, even the spectra for a completely regular orbit will be blurred into a collection of peaks of finite width, so that a relatively large number of frequencies are required to capture as much as 99% of the power, this corresponding to ϵ as small as 0.1. These considerations have led to the tentative identification of an optimal value $k \approx 0.9 - 0.95$. Within this limited range, the precise value is relatively unimportant since a typical rank correlation $\mathscr{R}(0.9, 0.95) \sim 0.96 - 0.98$.

It should also be noted that somewhat different definitions of complexity will yield very similar classifications. Suppose, e.g., that one defines another, related measure of the total complexity, namely $n' = (n_x n_y)^{1/2}$. When applied to the same ensemble of orbits, two alternative classifications based on n and n' will, for $k \approx 0.9 - 0.95$, typically yield a rank correlation $\mathscr{R}(n, n') \sim 0.95 - 0.99$. Significantly, however, it is important to use a definition involving some combination of n_x and n_y. For certain energies and potentials, rankings based individually on n_x or n_y will be correlated relatively strongly, with $\mathscr{R}(n_x, n_y)$ as large as 0.8 or more. In other cases, however, the values of n_x and n_y will be essentially uncorrelated.

In terms of quantities like $n(0.9)$ or $n(0.95)$, different segments of a single chaotic orbit of given energy can exhibit enormous diversity. Thus, e.g., an examination of 1024 different segments of length t_H, each evolved in the potential (3) with the same energy $E = -0.5$, yielded a mean $\langle n(0.9) \rangle = 56.2$ and a dispersion $\sigma(0.9) = 23.2$. The largest and smallest values of n ranged from 7 to 108. Alternatively, $\langle n(0.95) \rangle = 93.7$ and $\sigma(0.95) = 32.6$, the observed values now ranging from 20 to 155. Similarly, the lower energy $E = -0.6$ yielded $\langle n(0.9) \rangle = 44.8$ and $\sigma(0.9) = 24.6$, with different segments ranging from $n = 4$ to $n = 99$. Examples of particularly simple and complex or-

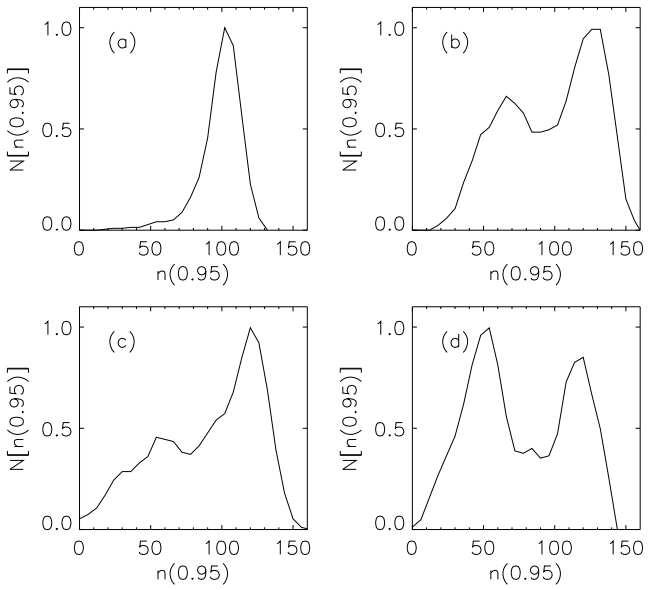

Fig. 3. a The distribution of complexities, $N[n(0.95)]$, for an ensemble of chaotic segments with $E = -0.3$ evolved in the potential (3) and sampled at intervals $\Delta t = t_H$. **b** The same for $E = -0.5$. **c** The same for $E = -0.55$. **d** The same for $E = -0.6$.

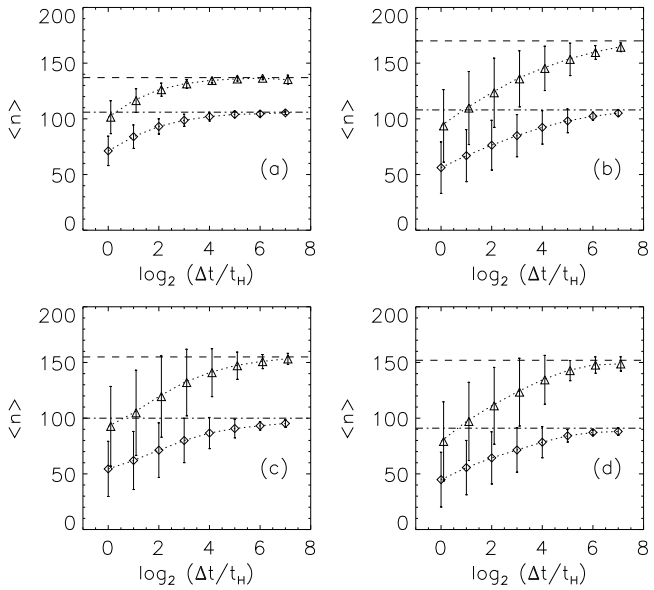

Fig. 4. a The mean complexities, $\langle n(0.95)\rangle$ (upper curve) and $\langle n(0.9)\rangle$ (lower curve), for ensembles of chaotic segments with $E = -0.3$, sampled at variable intervals $\Delta t = 2^k t_H$, with $k \leq 7$. **b** The same for $E = -0.5$. **c** The same for $E = -0.55$. **d** The same for $E = -0.6$.

bits are exhibited in Figs. 2, the nearly regular orbit having $n(0.9) = 14$ and $n(0.95) = 28$ and the wildly chaotic orbit having $n(0.9) = 90$ and $n(0.95) = 145$. The two left hand panels exhibit orbits in the $x - y$ plane. The two right panels exhibit the corresponding $|x(\omega)|$ and $|y(\omega)|$, normalised as in Figs. 1, the former represented by a solid curve and the latter by a dot-dashed curve.

The mean values $\langle n(0.9)\rangle$ and $\langle n(0.95)\rangle$ associated with segments of length t_H are much smaller than the complexities associated with longer time integrations that sample the invariant distribution. Thus, e.g., the invariant distributions exhibited in Figs. 1 are characterised by the following values: for $E = -0.3$, $n(0.9) = 106$ and $n(0.95) = 137$; for $E = -0.5$, $n(0.9) = 108$ and $n(0.95) = 170$; for $E = -0.55$, $n(0.9) = 100$ and $n(0.95) = 155$; and for $E = -0.6$, $n(0.9) = 91$ and $n(0.95) = 152$.

The form of the distribution of complexities, $N[n(k)]$, associated with an ensemble of segments sampling the same chaotic phase space region is also interesting. For the case of potentials, energies, and sampling intervals for which cantori are relatively unimportant and orbits can pass relatively unimpeded throughout the stochastic sea, one observes typically a singly peaked distribution which is well approximated as Gaussian. If, however, cantori play an important role, partitioning the chaotic phase space into relatively distinct regions, one typically observes instead a distribution of complexities which is more complicated in shape, seemingly comprised of two or more distinct populations. This diversity of behaviour is exhibited in Figs. 3, which exhibit the distributions $N[n(0.95)]$ for the potential (3), again allowing for the energies $E = -0.3$, -0.5, -0.55, and -0.6 and a sampling interval t_H.

As illustrated in Figs. 4, tracking the average complexity $\langle n(k)\rangle$ as a function of the sampling interval Δt can provide useful information about the rate at which an ensemble of chaotic orbits eventually approaches an invariant measure, characterised by invariant Fourier spectra. Each panel in this figure was constructed by (a) selecting several different chaotic orbits evolved in the potential (3) with the same energy E, each of total length $2^7 t_H = 128 t_H$, (b) partitioning each orbit into a collection of segments of variable length $2^k t_H$, with $k \leq 7$, (c) computing the complexity of each segment, and then (d) determining the mean and dispersion. The upper curve in each panel exhibits $\langle n(0.95)\rangle$; the lower curve exhibits $\langle n(0.9)\rangle$. The error bars attached to each point reflect the dispersion of each of the distributions $N[n(\Delta t)]$. The horizontal lines represent approximations to the complexity associated with the invariant distribution Γ, obtained by summing over all the segments of all the orbits. It is evident that the orbit segments with $E = -0.3$, analysed in Fig. 4a, approach a near-constant $\langle n\rangle$ much more rapidly than the other segments with $E = -0.5$, -0.55, and -0.6, which are exhibited in the remaining panels. This is a reflection of the fact that cantori are relatively unimportant in the chaotic phase space regions for $E = -0.3$, unlike the chaotic phase space regions at significantly lower energies where such obstructions can play an important role.

4. Correlations between complexity and exponential instability

Ordinary Lyapunov exponents can be defined as probing the average exponential instability of a chaotic orbit in an asymptotic $t \to \infty$ limit (cf. Benettin et al. 1976). By analogy (cf. Grasssberger et al. 1988, Sepúlveda et al. 1989) one can also

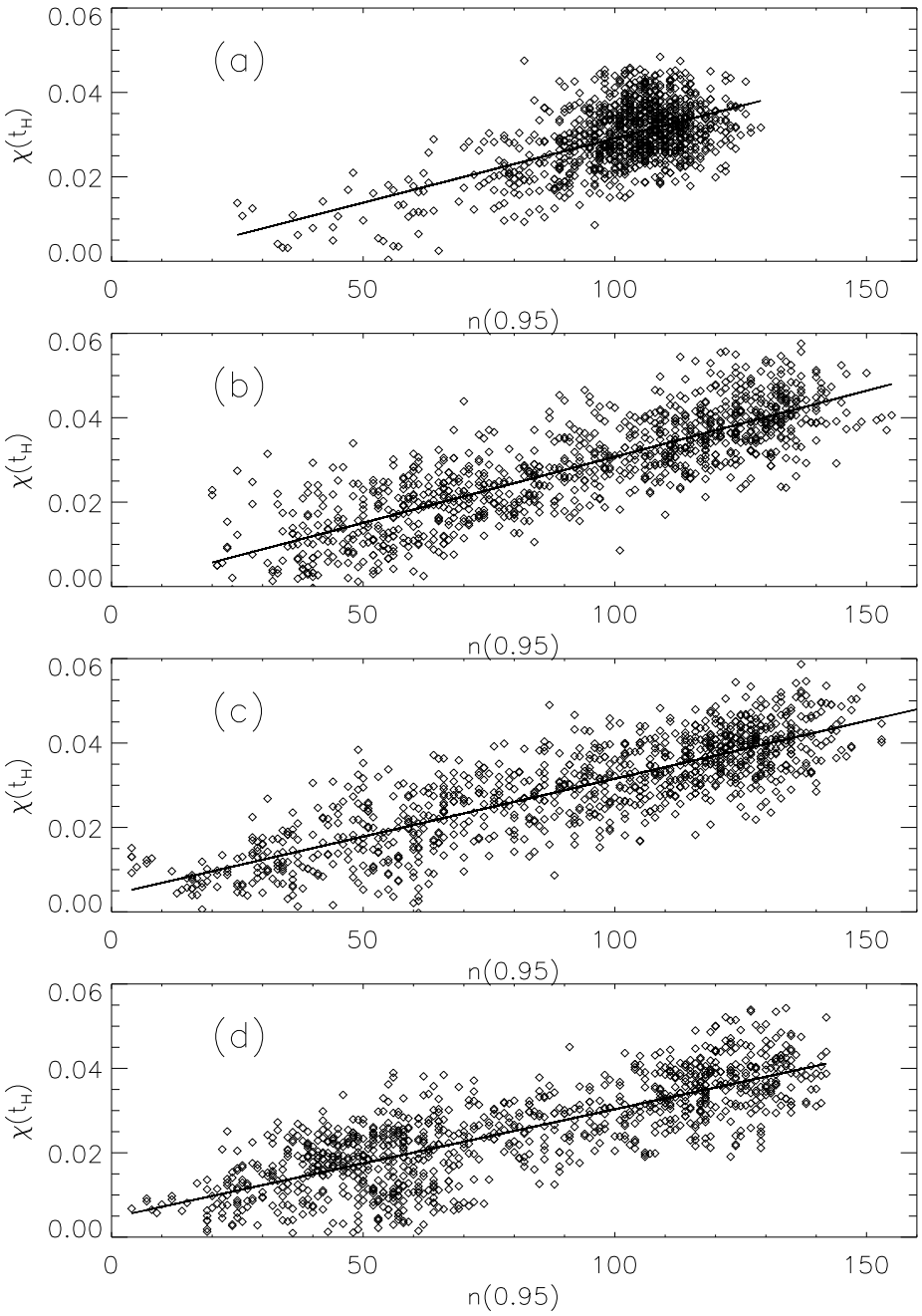

Fig. 5. a A scatter plot of χ vs. $n(0.95)$ for 1024 chaotic orbit segments of energy $E = -0.4$ evolved in the potential (3), generated by partitioning 8 orbits of length $128t_H$ into segments of length $\Delta t = t_H$. **b** The same for $E = -0.5$. **c** The same for $E = -0.55$. **d** The same for $E = -0.6$.

define *short time Lyapunov exponents* as probes of the exponential instability of finite segments of a chaotic orbit. Specifically, given some infinitesimal phase space perturbation $\delta Z(0)$, one can identify a short time exponent

$$\chi(t) \equiv \lim_{\delta Z(0)\to 0} \frac{1}{t} \ln \left[\frac{\|\delta Z(t)\|}{\|\delta Z(0)\|} \right], \tag{5}$$

where $\| \, . \, \|$ denotes an appropriate norm.

For generic initial perturbations, this $\chi(t)$ will converge towards the maximum ordinary Lyapunov exponent in a $t \to \infty$ limit, independent of the choice of norm or the particular value of $\delta Z(0)$. However, for finite times the computed $\chi(t)$ will depend on both $\delta Z(0)$ and the assumed norm. Suppose, therefore, for specificity, that $\| \, . \, \|$ is taken to be the natural Euclidean norm. It is then clear that, if one focuses on time intervals long compared with the characteristic time scale associated with the average exponential instability, the computed $\chi(t)$ will be nearly independent of the initial $\delta Z(0)$, closely approximating the effects of an initial perturbation oriented in the most unstable phase space direction. It follows, therefore, that, for sufficiently long time intervals t, approximations to the largest, or maximal, short time Lyapunov exponent can be obtained in the usual fashion by tracking the evolution of some arbitrarily chosen initial $\delta Z(0)$, implementing at regular intervals a renormalisation to prevent $\delta Z(t)$ from becoming too large.

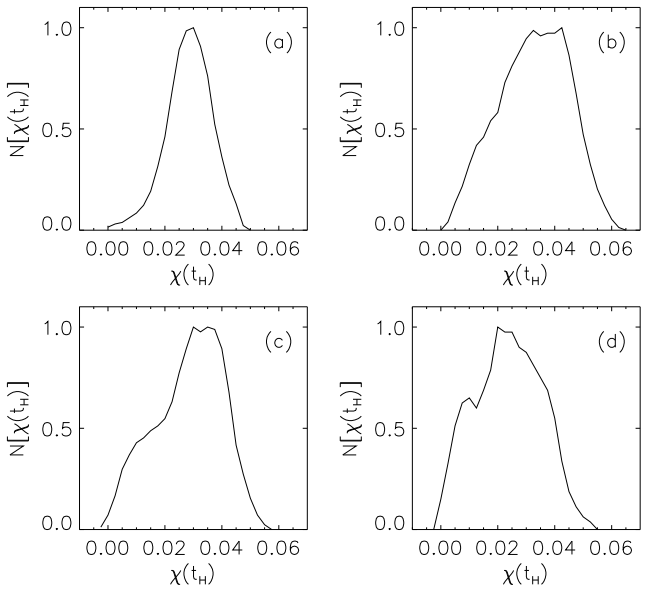

Fig. 6. a The distribution of short time Lyapunov exponents, $N[\chi]$, for an ensemble of chaotic segments with $E = -0.3$ evolved in the potential (3) and sampled at intervals $\Delta t = t_H$. **b** The same for $E = -0.5$. **c** The same for $E = -0.55$. **d** The same for $E = -0.6$.

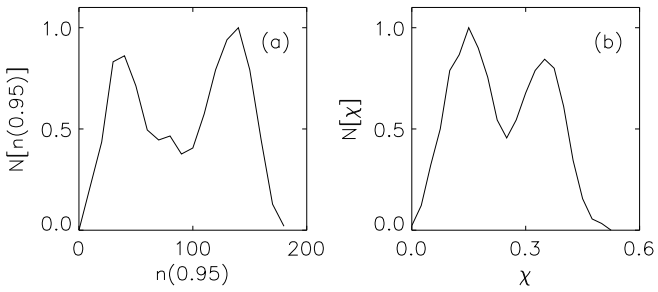

Fig. 7. a The distribution of complexities, $N[n(0.95)]$, for an ensemble of chaotic segments with $E = 20$ evolved in the truncated Toda potential and sampled at intervals $\Delta t \approx 2.5 t_H$. **b** The distribution of short time Lyapunov exponents, $N[\chi]$, associated with the same ensemble.

The same line of reasoning indicates that, if a single initial condition is integrated for a long period and a running $\chi(t)$ is recorded at fixed, uniformly spaced intervals Δt, the resulting collection of χ's can be analysed to extract a collection of short time Lyapunov exponents for the successive intervals. Specifically, one can extract a short time exponent χ for the $(k+1)$th segment, extending from $t_k = k\Delta t$ to $t_k + \Delta t$ by the natural definition (Kandrup & Mahon 1994b)

$$\chi(\Delta t_k) \equiv \frac{(t_k + \Delta t)\chi(t_k + \Delta t) - t_k \chi(t_k)}{\Delta t}. \qquad (6)$$

Earlier papers (cf. Mahon et al. 1995) have shown that characterisations of chaotic segments based on short time Lyapunov exponents can provide useful information about phase space transport in a complex phase space. The obvious question is whether and, if so, to what extent such characterisations coincide with characterisations based on the notion of complexity defined in Sect. 3.

This issue was considered in detail for chaotic orbits with several different energies evolving in the potential (3), allowing in the first instance for a basic sampling interval $\Delta t = t_H$. For each energy, eight different initial conditions were evolved for a total time $128 t_H$ and then partitioned into segments of length t_H. For each segment, the complexity was computed using the prescription introduced in Sect. 3 and a short time Lyapunov exponent χ was derived using Eqs. (5) and (6). Figs. 5 exhibit scatter plots for the 1024 resulting values of χ and $n(0.95)$ for four different energies, $E = -0.3, -0.5, -0.55$, and -0.6. The solid curves superimposed represent least squares linear fits. It is obvious that, for all four energies, there is a strong direct correlation between χ and $n(0.95)$ which is consistent, visually, with a linear trend. Allowing for a quadratic correction to this linear fit decreases the residuals by less than $\sim 1\%$, but this is hardly surprising in view of the fact that the plots exhibit significant scatter. More significantly, for the two intermediate energies, where the full range of values of $n(0.95)$ is sampled the most uniformly, allowing for a quadratic correction only changes the best fit value of the linear coefficient by $\sim 5\%$.

To quantify this trend more precisely, one can also compute rank correlations $\mathscr{R}(\chi, n(k))$ between χ and $n(k)$. Thus, e.g., for $E = -0.5$, $\mathscr{R}(\chi, n(0.95)) = 0.835$ and $\mathscr{R}(\chi, n(0.9)) = 0.818$; for $E = -0.55$, $\mathscr{R}(\chi, n(0.95)) = 0.814$ and $\mathscr{R}(\chi, n(0.9)) = 0.808$; and for $E = -0.6$, $\mathscr{R}(\chi, n(0.95)) = 0.791$ and $\mathscr{R}(\chi, n(0.9)) = 0.801$. For the higher energy $E = -0.3$, the rank correlations are much weaker, namely $\mathscr{R}(\chi, n(0.95)) = 0.439$ and $\mathscr{R}(\chi, n(0.9)) = 0.406$. However, this is easily understood as a reflection of the fact that, for this energy, the overwhelming majority of the points are clustered near $n(0.9) \sim 80$, $n(0.95) \sim 110$, and $\chi \sim 0.3$, with relatively few points at much lower (or higher) values. It follows that the data set does not come close to providing a broad sampling of a trend that extends over a large range of n and χ. Significantly, however, even though the rank correlation for $E = -0.3$ is much smaller than for the lower energies, there would still appear to be an obvious trend. For all four values of energy, this correlation also persists if χ is compared with $n(k)$ for lower values of k, although the correlation becomes significantly weaker for $k < 0.6$ or so.

Given the existence of this apparent near-linear correlation between n and χ, one might expect that the distribution of short time Lyapunov exponents, $N[\chi]$, would be closely related to the distributions of complexities, $N[n]$, described in Sect. 3. The extent to which this is true is illustrated in Figs. 6, which exhibit the distribution of short time Lyapunov exponents, $N[\chi(t_H)]$, for the same segments that were used to generate the distributions $N[n(0.95)]$ exhibited in Figs. 3.

Like $N[n(0.95)]$, the distribution of short time Lyapunov exponents, $N[\chi]$, for $E = -0.3$ is approximately Gaussian, which is consistent with the apparent fact that the chaotic phase space at this energy is dominated by a single population. However, the distributions of short time exponents at lower energies are significantly more complicated, this reflecting the fact that, over time scales $\sim t_H$, chaotic orbits at a given energy are par-

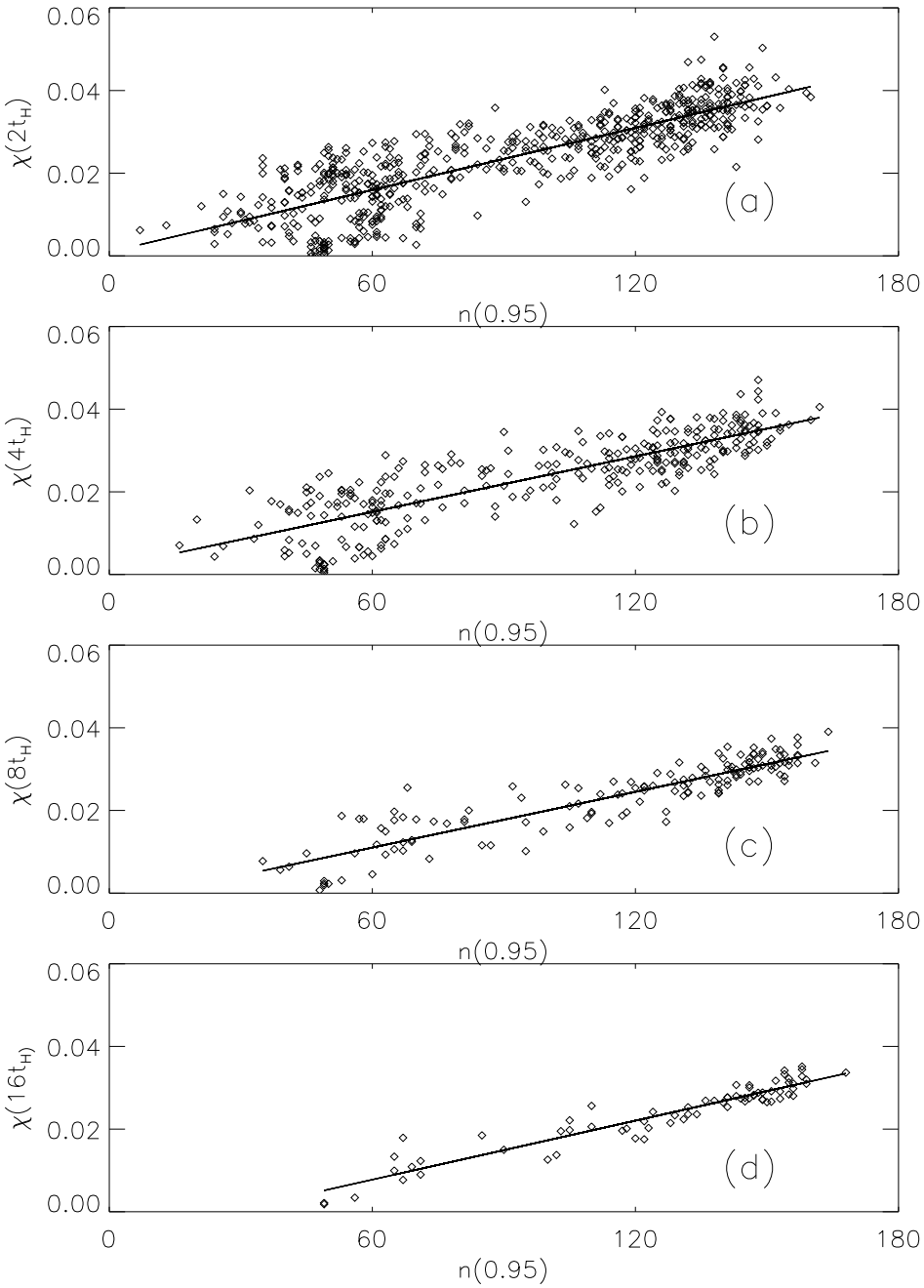

Fig. 8. a A scatter plot of χ vs. $n(0.95)$ for the segments shown in Fig. 5d, now sampled at an interval $\Delta t = 2t_H$. **b** The same for $\Delta t = 4t_H$. **c** The same for $\Delta t = 8t_H$. **d** The same for $\Delta t = 16t_H$.

titioned into several nearly distinct populations (cf. Mahon et al. 1995). In this sense, the distributions of complexities and short time Lyapunov exponents are in agreement. It is, however, significant that the distributions of complexities show more obvious structure than do the corresponding distributions of short time exponents.

This would suggest that complexities may perhaps prove more sensitive tools for orbit classification than are short time Lyapunov exponents, a result corroborated by investigations of the dihedral and truncated Toda potentials discussed in Sect. 1. This is, e.g., illustrated in Figs. 7a and 7b which exhibit, respectively, the distributions $N[n(0.95)]$ and $N[\chi]$ for 1024 chaotic orbits with energy $E = 20$ evolved in the sixth order truncation of the Toda potential, the basic time interval now corresponding to $\Delta t = 256 \approx 2.5t_H$. For this ensemble of orbit segments, the rank correlation $\mathscr{R}(\chi, n(0.95)) = 0.794$. Both distributions are obviously bimodal, but the two peaks in $N[n(0.95)]$ are more clearly separated.

The basic interpretation is simple: For relatively low energies and sampling times as short as t_H, chaotic orbit segments generated in the potential (3) divide naturally into several distinct populations, each characterised by a singly peaked distribution of short time Lyapunov exponents and a singly peaked distribution of complexities. The individual distributions of short time exponents are sufficiently broad that, when combined to yield the total $N[\chi(t_H)]$, much of the structure is lost. However,

the individual distributions of complexities are narrower so that, when combined, more of the original structure remains.

The final point to be stressed is that the strong correlation between χ and n described above does not rely critically on the specific sampling interval Δt. Rather, such correlations would appear to arise for any ensemble of orbit segments where both n and χ vary over a significant range. This is illustrated in Figs. 8, which were derived from the same integrations used in Fig. 5d, but now allowing for sampling intervals of length $\Delta t = 2t_H$, $4t_H$, $8t_H$, and $16t_H$.

Short time Lyapunov exponents and the complexity of Fourier spectra provide two complementary tools with which to probe the degree of chaos exhibited by chaotic orbit segments. The complexity quantifies the degree to which the segment can be approximated as multiply periodic with only a few periodicities; short time Lyapunov exponents probe the degree to which the segment is unstable towards small changes in initial conditions. The principal conclusion of this paper is that there exists a strong, nearly linear, correlation between these two different probes of chaos.

The existence of this correlation makes sense intuitively, given that broad band Fourier spectra and sensitive dependence on initial conditions have both been used to provide operational definitions of chaos. However, as exhibited, e.g., by the significant dispersions in Fig. 5, the correlation is not perfect. Only in an asymptotic $t \to \infty$ limit does it seem possible to speak of a unique complexity and a unique maximum Lyapunov exponent, both of which seem independent of the detailed choice of initial conditions within a connected phase space region.

One possible use of complexities and short time Lyapunov exponents is as tools to track phase space transport, e.g., diffusion through cantori in two-dimensional Hamiltonian systems, the key point being that orbit segments trapped near regular regions tend to have smaller complexities and smaller short time exponents than do segments travelling unimpeded throughout the stochastic sea. However, neither tool is ideal for tracking phase space transport for individual orbits since, even in a given finite phase space region, the complexities and short time Lyapunov exponents vary significantly. Nevertheless, both tools *can* be extremely useful when applied to orbit ensembles, where the existence of distinct phase space populations can be manifested by multiply peaked distributions.

Given the near-linear correlation between complexities and short time Lyapunov exponents, one would not expect that either tool is fundamentally better than the other. Rather, these tools provide two alternative ways in which to analyse the same orbit segments. However, what *is* clear is that computing Fourier spectra for uniform samplings of an orbit segment is in general less costly computationally than computing short time Lyapunov exponents, which involves evaluating both the true orbit and a linearised perturbation thereof.

Acknowledgements. HEK acknowledges useful discussions with Haywood Smith. Some of the computations were facilitated by computer time made available through the Research Computing Initiative at the Northeast Regional Data Center (Florida) by IBM Corp. HEK was supported in part by the NSF grant PHY92-03333. BLE was supported by NASA through the Florida Space Grant Consortium.

References

Armbruster, D., Guckenheimer, J., Kim, S., 1989. Phys. Lett. A 140, 416
Arnold, V. I., 1964. Russian Math. Surveys 18, 85
Aubry, S., Andre, G., 1978. in: Solitons and Condensed Matter Physics, ed. Bishop, A. R., Schneider, T. Springer, Berlin
Benettin, G., Galgani, L., Strelcyn, J.-M., 1976. Phys. Rev. A 14, 2338
Grassberger, P., Badii, R., Poloti, A., 1988. J. Stat. Phys. 51, 135
Hasan, H., Norman, C., 1990. ApJ 361, 69
Kandrup, H. E., Bradley, B. O., 1995. preprint
Kandrup, H. E., Eckstein, B. L., 1996. Ann. N. Y. Acad. Sci., in press
Kandrup, H. E., Mahon, M. E., 1994a. Phys. Rev. E 49, 3735
Kandrup, H. E., Mahon, M. E., 1994b. A&A 290, 762
Lichtenberg, A. J., Lieberman, M. A., 1992. Regular and Chaotic Dynamics. Springer, Heidelberg
Mahon, M. E., Abernathy, R. A., Bradley, B. O., Kandrup, H. E., 1995. MNRAS 275, 443
Mather, J. N., 1982. Topology 21, 45
Press, W. H., Flannery, B. P., Teukolsky, S. A., Vetterling, 1992. Numerical Recipes in C. 2nd edition. Cambridge University Press, Cambridge
Sepúlveda, M. A., Badii, R., Pollak, E., 1989. Phys. Rev. Lett. 63, 1226
Tabor, M., 1989. Chaos and Integrability in Nonlinear Dynamics. Wiley, New York
Toda, M., 1967. J. Phys. Soc. Japan 22, 431

This article was processed by the author using Springer-Verlag LaTeX A&A style file *L-AA* version 3.